

# UC San Diego

## UC San Diego Previously Published Works

### Title

Quantitative ultrashort echo time MR imaging of knee osteochondral junction: An ex vivo feasibility study

### Permalink

<https://escholarship.org/uc/item/41k3z98r>

### Journal

NMR in Biomedicine, 37(12)

### ISSN

0952-3480

### Authors

Athertya, Jiyo S

Suprana, Arya

Lo, James

et al.

### Publication Date




2024-12-01

### DOI

10.1002/nbm.5253

Peer reviewed

# Quantitative ultrashort echo time MR imaging of knee osteochondral junction: An ex vivo feasibility study

Jiyo S. Athertya<sup>1</sup>  | Arya Suprana<sup>1,2</sup> | James Lo<sup>1,2</sup> | Alecio F. Lombardi<sup>1,3</sup>  |  
Dina Moazamian<sup>1</sup>  | Eric Y. Chang<sup>1,3</sup> | Jiang Du<sup>1,2,3</sup> | Yajun Ma<sup>1</sup>

<sup>1</sup>Department of Radiology, University of California San Diego, San Diego, California, USA

<sup>2</sup>Department of Bioengineering, University of California San Diego, San Diego, California, USA

<sup>3</sup>Radiology Service, Veterans Affairs San Diego Healthcare System, San Diego, California, USA

## Correspondence

Yajun Ma, Department of Radiology, University of California, San Diego, 9452 Medical Center Dr., San Diego, CA 92037, USA.

Email: [yam013@health.ucsd.edu](mailto:yam013@health.ucsd.edu)

## Funding information

National Institutes of Health, Grant/Award Numbers: R01AR062581, R01AR068987, R01AR075825, R01AR078877, R01AR079484, P30AR073761, R21AR075851, F32AG082458; U.S. Department of Veterans Affairs; VA Clinical Science Research & Development Service, Grant/Award Numbers: I01CX001388, I01CX000625; GE Healthcare

## Abstract

Compositional changes can occur in the osteochondral junction (OCJ) during the early stages and progressive disease evolution of knee osteoarthritis (OA). However, conventional magnetic resonance imaging (MRI) sequences are not able to image these regions efficiently because of the OCJ region's rapid signal decay. The development of new sequences able to image and quantify OCJ region is therefore highly desirable. We developed a comprehensive ultrashort echo time (UTE) MRI protocol for quantitative assessment of OCJ region in the knee joint, including UTE variable flip angle technique for  $T_1$  mapping, UTE magnetization transfer (UTE-MT) modeling for macromolecular proton fraction (MMF) mapping, UTE adiabatic  $T_{1\rho}$  (UTE-Adiab $T_{1\rho}$ ) sequence for  $T_{1\rho}$  mapping, and multi-echo UTE sequence for  $T_2^*$  mapping.  $B_1$  mapping based on the UTE actual flip angle technique was utilized for  $B_1$  correction in  $T_1$ , MMF, and  $T_{1\rho}$  measurements. Ten normal and one abnormal cadaveric human knee joints were scanned on a 3T clinical MRI scanner to investigate the feasibility of OCJ imaging using the proposed protocol. Volumetric  $T_1$ , MMF,  $T_{1\rho}$ , and  $T_2^*$  maps of the OCJ, as well as the superficial and full-thickness cartilage regions, were successfully produced using the quantitative UTE imaging protocol. Significantly lower  $T_1$ ,  $T_{1\rho}$ , and  $T_2^*$  relaxation times were observed in the OCJ region compared with those observed in both the superficial and full-thickness cartilage regions, whereas MMF showed significantly higher values in the OCJ region. In addition, all four UTE biomarkers showed substantial differences in the OCJ region between normal and abnormal knees. These results indicate that the newly developed 3D quantitative UTE imaging techniques are feasible for  $T_1$ , MMF,  $T_{1\rho}$ , and  $T_2^*$  mapping of knee OCJ, representative of a promising approach for the evaluation of compositional changes in early knee OA.

## KEYWORDS

knee joint, osteochondral junction, quantitative, ultrashort echo time

**ABBREVIATIONS:** ACL, anterior cruciate ligament; AFC, anterior femoral condyle; AFI, actual flip angle; AFP, adiabatic full passage; ICC, intraclass correlation coefficient; IFC, inferior femoral condyle; MMF, macromolecular proton fraction; OCJ, osteochondral junction; PD-FSE, proton density-weighted fast spin echo; PFC, posterior femoral condyle; ROI, region of interest; TP, tibial plateau; UTE, ultrashort echo time; UTE-MT, UTE magnetization transfer.

Jiyo S. Athertya and Arya Suprana contributed equally to this work.

## 1 | INTRODUCTION

Osteoarthritis (OA) is a common joint disorder that causes functional disability in older adults. It is the most prevalent type of arthritis in adult populations, with more than 32.5 million diagnoses in the United States alone. OA involves both degradation of individual tissue components and failure of the joint system as a whole.<sup>1</sup> By the late stages, it is typically characterized by degeneration of articular cartilage, synovial inflammation, and changes in periarticular and subchondral bone.<sup>2</sup>

The osteochondral junction (OCJ) is an emerging area of interest in OA pathogenesis. It comprises the region between the deep layer of articular cartilage and the underlying subchondral bone, including the deep zone cartilage, the zone of calcified cartilage, and the subchondral bone plate.<sup>3</sup> These layers of the OCJ interact synergistically with each other to form a complex foundational basis for joint's load-bearing function.<sup>4</sup> In OA, the zone of calcified cartilage advances toward the deep zone of uncalcified cartilage. Additionally, the tidemark, which is the boundary between the calcified and uncalcified cartilage, undergoes duplication. The formation of new tidemarks indicates ongoing remodeling processes in the deep cartilage, a hallmark of OA.<sup>5</sup> This phenomenon may be attributed to the increasing vascular invasion from the marrow space into the overlying calcified and noncalcified cartilage regions.<sup>6–8</sup> Recent studies have identified changes in the OCJ as a potential marker for early OA detection.<sup>9–11</sup>

Magnetic resonance imaging (MRI) is an important tool for the non-invasive assessment of OA because of the technique's excellent soft tissue contrast.<sup>12</sup> Clinical MRI can detect not only cartilage degeneration and bone marrow lesions but also synovial inflammation, meniscal tears, and ligament injuries. Recent developments in quantitative MRI methodologies, such as  $T_{1\rho}$ <sup>13,14</sup> and  $T_2$ <sup>15</sup> mapping, have revealed alterations in tissue composition associated with OA, namely, changes in collagen and proteoglycan content. Magnetization transfer (MT) imaging has been employed for indirect assessment of macromolecules in biological tissues.<sup>16–18</sup> However, the rapid signal decay characteristic of OCJ regions has rendered conventional MRI sequences incapable of assessing these areas, thus limiting the techniques' translational potential for early OA detection.<sup>19</sup>

Ultrashort echo time (UTE) sequences have been developed to directly image and quantify tissues with short  $T_2$  relaxation times, such as bone, tendon, ligament, and myelin.<sup>20–22</sup> Both 2D and 3D UTE techniques have been used to study the OCJ regions in the knee.<sup>19,23–25</sup> The 3D UTE sequence has been demonstrated to be more suitable for high-resolution imaging of the OCJ compared with its single-slice 2D UTE sequence counterpart because of 3D's advantages with respect to whole knee coverage capability, reduced partial volume effect, and decreased sensitivity to eddy currents.<sup>26</sup> Recently, several 3D UTE methods have been developed for morphological imaging of the OCJ with high contrast in whole knee, including UTE dual echo subtraction,<sup>27</sup>  $T_1$ -weighted fat saturated UTE,<sup>28</sup> inversion recovery prepared fat saturated UTE,<sup>29</sup> and dual inversion recovery prepared UTE.<sup>30</sup> In order to highlight the short  $T_2$  OCJ regions, these techniques selectively suppress signals from the long  $T_2$  fat and more superficial cartilage regions. 3D quantitative UTE techniques have also been applied, mainly using UTE  $T_2^*$ , to assess compositional changes in the OCJ before and after anterior cruciate ligament (ACL) reconstruction,<sup>31,32</sup> with elevated UTE  $T_2^*$  values in the OCJ observed following such surgeries.

In this study, we aimed to develop a comprehensive 3D UTE imaging protocol, including the UTE variable flip angle (UTE-VFA) technique for  $T_1$  mapping,<sup>33,34</sup> UTE magnetization transfer modeling (UTE-MT) for macromolecular proton fraction (MMF) mapping,<sup>17,35</sup> UTE adiabatic  $T_{1\rho}$  (UTE-Adiab $T_{1\rho}$ ) sequence for  $T_{1\rho}$  mapping,<sup>36,37</sup> and multi-echo UTE sequence for  $T_2^*$  mapping,<sup>38</sup> for quantitative assessment of the OCJ region in the whole knee joint.  $B_1$  mapping based on the UTE actual flip angle (UTE-AFI) technique was utilized for  $B_1$  correction in  $T_1$ , MMF, and  $T_{1\rho}$  mapping.<sup>34,39</sup> In this scanning protocol, biochemical components including water, collagen, and proteoglycan were assessed by UTE biomarkers  $T_1$ ,  $T_2^*/\text{MMF}$ , and  $T_{1\rho}$ , respectively. Moreover, it has previously been demonstrated that  $T_1$ , MMF, and Adiab $T_{1\rho}$  exhibit minimal sensitivity to the magic angle effect. This property is essential for the study of collagen-rich tissues, including the OCJ.<sup>40–43</sup> To investigate the feasibility of quantitative OCJ imaging using the proposed protocol, 10 normal and one abnormal cadaveric human knee joints were scanned on a 3T clinical MRI scanner. Quantitative UTE measures of the OCJ region were also compared between full cartilage and superficial cartilage regions.

## 2 | METHODS

### 2.1 | Sample preparation

Institutional review board approval was received for this study. Ten normal knee joints (aged 38–72 years, mean age  $48 \pm 10$  years; 6 males, 4 females) and one abnormal (88 years old, male) cadaveric human knee joint were scanned to investigate the feasibility of OCJ imaging using the proposed protocol. These knee joint specimens were stored in a  $-80^\circ$  freezer and thawed in a water bath for  $\sim 24$  h before scanning. All scans were performed at room temperature.

## 2.2 | MR data acquisition

The 11 ex vivo whole knee joint specimens were scanned on a 3T GE MR750 scanner (GE Healthcare Technologies, Milwaukee, WI, USA) with an eight-channel knee coil for both radiofrequency transmission and signal reception. Diagrams of major sequences of the proposed quantitative UTE protocol are shown in Figure 1, including UTE-AFI, UTE-MT, UTE-AdiabT<sub>1p</sub>, and multi-echo UTE. Volumetric B<sub>1</sub> maps were produced by the UTE-AFI technique and applied to correct B<sub>1</sub> inhomogeneity in T<sub>1</sub>, T<sub>1p</sub>, and MMF quantification.<sup>34,39</sup> This UTE-AFI sequence included acquiring two UTE datasets at different TRs in an interleaved manner (Figure 1A). The UTE-VFA technique was employed to facilitate T<sub>1</sub> quantification (sequence not shown).<sup>34</sup> Two-pool MT modeling was performed on a series of UTE-MT acquisitions with different MT powers and frequency offsets (Figure 1B).<sup>35</sup> The UTE-AdiabT<sub>1p</sub> technique utilized a train of identical non-selective adiabatic full passage (AFP) pulses with a duration of 6.048 ms, bandwidth of 1.643 kHz, and maximum B<sub>1</sub> amplitude of 17 μT to generate T<sub>1p</sub> contrast (Figure 1C).<sup>37</sup> For improved scan efficiency, multi-spoke acquisitions were employed after each MT or AdiabT<sub>1p</sub> preparation. Multi-echo UTE sequence was utilized for T<sub>2</sub><sup>\*</sup> measurement (Figure 1D).<sup>38</sup> The fundamental 3D UTE sequence employed for data acquisition in the proposed UTE imaging protocol was comprised of a short rectangular pulse for signal excitation followed by 3D cone trajectory for efficient k-space coverage.<sup>44</sup>

The field of view, matrix size, bandwidth, and total scan time for each ex vivo knee joint scan were 15 × 15 × 8 cm<sup>3</sup>, 256 × 256 × 40, 125 kHz, and 90 min, respectively. Other sequence parameters of the quantitative UTE imaging protocols were (A) 3D UTE-AFI sequence: TR<sub>1</sub>/TR<sub>2</sub>/TE = 20/100/0.032 ms and flip angle (FA) = 45°; (B) 3D UTE-VFA sequence: FAs = 5°, 10°, 20°, and 30°, and TR/TE = 20/0.032 ms; (C) 3D UTE-MT sequence: MT pulse FAs = 500°, 1000°, and 1500°, MT pulse frequency offsets = 2, 5, 10, 20, and 50 kHz, TR/TE = 100/0.032 ms, FA = 7°, number-of-spokes per-TR (N<sub>sp</sub>) = 9, and spoke interval (τ) = 6 ms; (D) 3D UTE-AdiabT<sub>1p</sub> sequence: spin lock times (TSLs) = 0, 12, 24, 36, 48, 72, and 96 ms corresponding to the number of AFP pulses = 0, 2, 4, 6, 8, 12, and 16, TR/TE = 500/0.032 ms, FA = 10°, N<sub>sp</sub> = 21, and τ = 6 ms; and (E) 3D multi-echo UTE sequence with an echo train of six: TEs = 0.032, 4.4, 8.8, 13.2, 22, and 35.2 ms, TR = 48 ms, and FA = 10°. The clinical proton density-weighted fast spin echo (PD-FSE) and fat-suppressed T<sub>2</sub>-weighted FSE (T<sub>2</sub>-FSE) sequences were also scanned for clinical diagnosis with the following sequence parameters: (A) PD-FSE: TR/TE = 3800/31 ms and (B) T<sub>2</sub>-weighted FSE: TR/TE = 8821/71.5 ms.

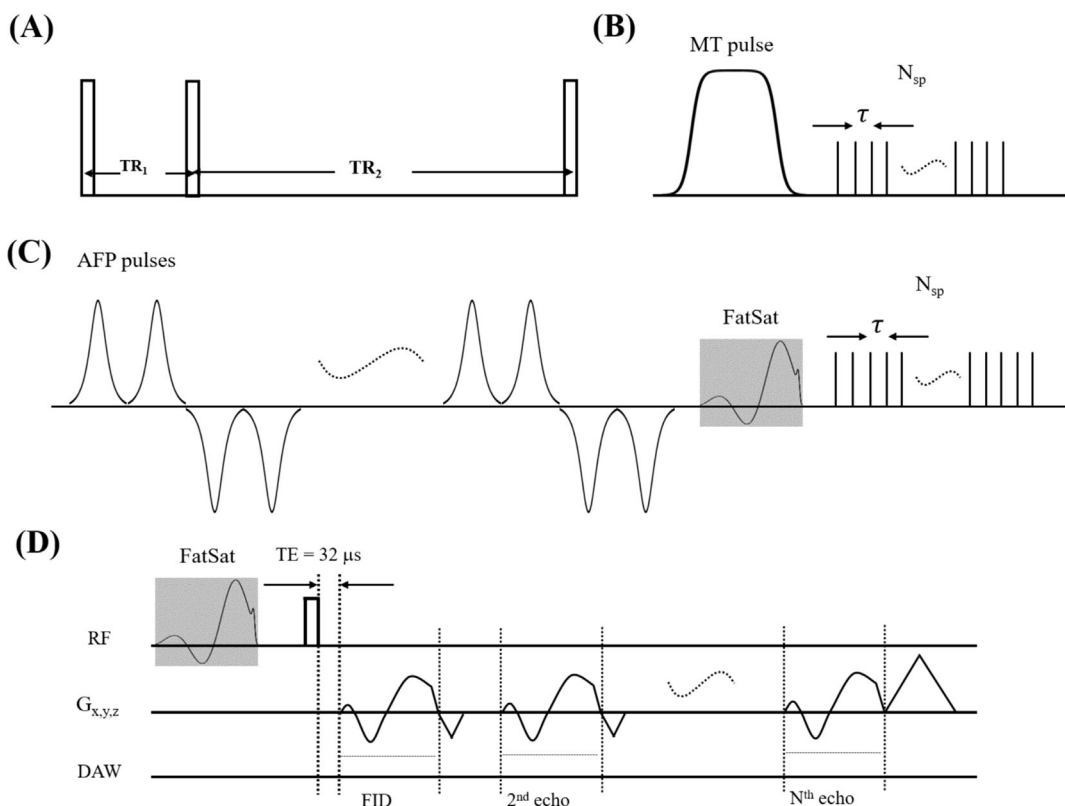


**FIGURE 1** Diagrams of quantitative 3D UTE sequences. The UTE-AFI sequence with interleaved TRs is used to measure the B<sub>1</sub> inhomogeneity (A). A Fermi pulse with a duration of 8 ms and a bandwidth of 160 Hz is used to saturate the magnetization of the macromolecular proton pool to generate the MT contrast in UTE-MT (B). A train of AFP pulses (hyperbolic secant shape, duration of 6.048 ms, and bandwidth of 1.643 kHz) is used to lock the spin to generate the T<sub>1p</sub> contrast in UTE-AdiabT<sub>1p</sub> (C). A multi-echo UTE sequence is used for T<sub>2</sub><sup>\*</sup> measurement (D). Fat saturation (FatSat) is applied to UTE-AdiabT<sub>1p</sub> and multi-echo UTE sequences for fat suppression.

## 2.3 | Data analysis

As seen in Figure 2, the OCJ region shows high signal intensities on the UTE-VFA image with a flip angle of  $30^\circ$ . This is because the OCJ region has much shorter  $T_1$  relaxation times than the superficial cartilage regions, making the short  $T_1$  tissue bright on the highly  $T_1$ -weighted image.<sup>28</sup> In this study, the following regions of interest (ROIs) were manually drawn on these highly  $T_1$ -weighted UTE images (i.e., UTE-VFA images with a flip angle of  $30^\circ$ ) for each knee joint by two well-trained readers: OCJ, superficial and full thickness cartilage regions for four different parts, namely, the anterior femoral condyle (AFC), inferior femoral condyle (IFC), posterior femoral condyle (PFC), and tibial plateau (TP) (Figure 2). A total of 12 ROIs were obtained for each specimen, consisting of three zones (OCJ, superficial cartilage, and full cartilage) across four different regions (AFC, IFC, PFC, and TP). The  $T_1$ , MMF,  $T_{1p}$ , and  $T_2^*$  parameter mapping for all ROIs was performed using the Levenberg–Marquardt algorithm for nonlinear least-square curve fitting.<sup>45,46</sup> All data processing codes were programmed in MATLAB (Mathworks Inc., Natick, MA, USA).

## 2.4 | Statistical analysis

After data processing, statistical analysis was performed using SPSS 28.0 software (IBM, Armonk, NY, USA). Intraclass correlation coefficient (ICC) was computed to investigate the reliability of the ROI drawings between both readers. The Kolmogorov–Smirnov test was applied to the dataset to check for normality. A paired  $t$ -test was performed on all the quantitative UTE biomarkers between different regions (i.e., OCJ, full cartilage, and superficial cartilage) in normal knee joints. Bonferroni's correction for multiple comparisons was applied to the 48 tests (three pairwise comparisons of layers for four biomarkers in four different knee parts), with  $p$ -values  $<0.001$  considered statistically significant.

## 3 | RESULTS

Figure 3 shows the representative clinical images and quantitative UTE images for a normal knee joint sample. The clinical PD-FSE and  $T_2$ -FSE images presented much lower signals in the OCJ region than the UTE images due to the former's relatively longer TE values. As expected, a high

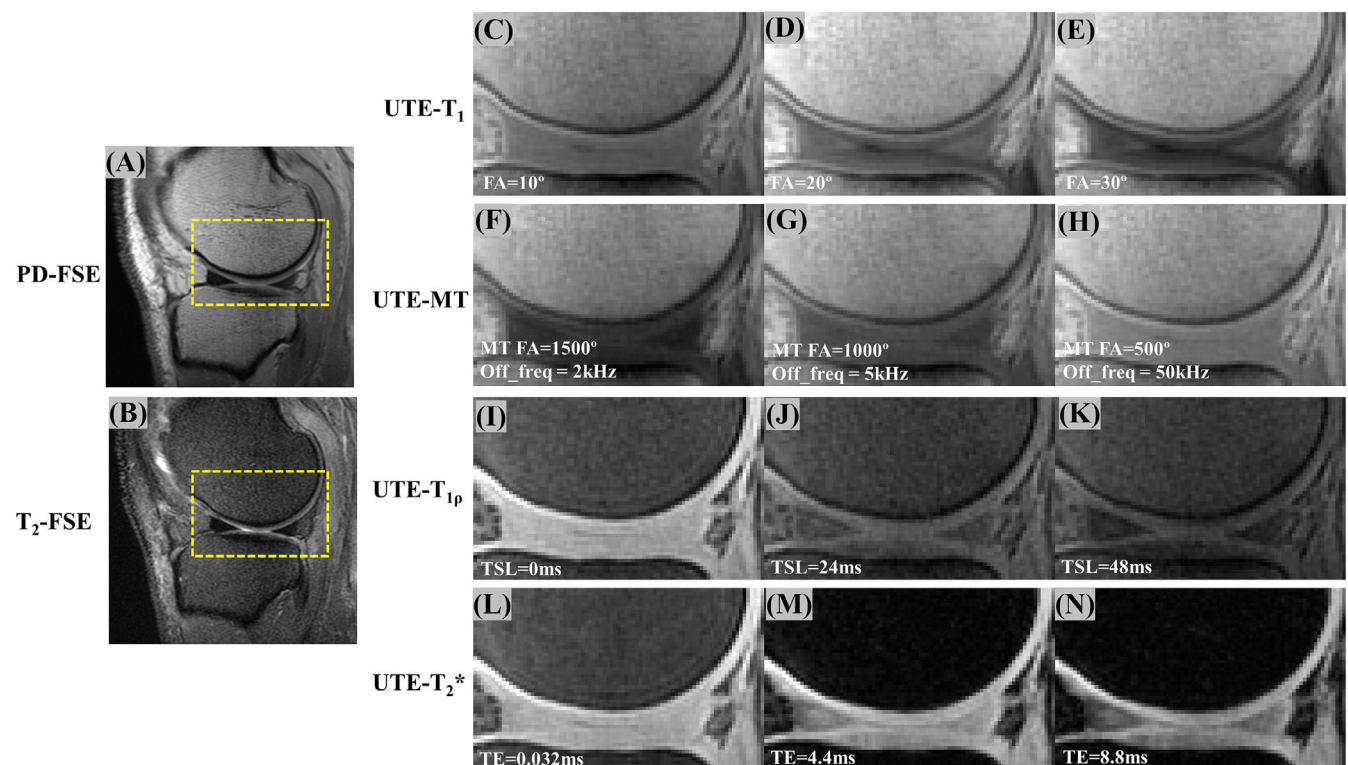


**FIGURE 2** Representative clinical (A–B) and quantitative UTE (C–N) images from a 45-year-old male donor. The OCJ regions are dark in the clinical PD-FSE (A) and  $T_2$ -FSE (B) images. The zoomed UTE images of the region inside of the yellow boxes (seen in A and B) show OCJ contrasts with four different techniques, including UTE- $T_1$  (FAs of  $10^\circ$  (C),  $20^\circ$  (D), and  $30^\circ$  (E)), UTE-MT (MT FA =  $1500^\circ$  and frequency offset = 2 kHz (F), MT FA =  $1000^\circ$  and frequency offset = 5 kHz (G), and MT FA =  $500^\circ$  and frequency offset = 50 kHz (H)), UTE- $T_{1p}$  (TSLs of 0 (I), 24 (J), and 48 ms (K)), and UTE- $T_2^*$  (TEs of 0.032 (L), 4.4 (M), and 8.8 ms (N)).

OCJ contrast was found in the UTE-VFA images with high FAs. Tissue signal attenuation was observed in the UTE-MT images with a strong MT effect (i.e., a high MT FA or a low-frequency offset). Signal decay in the cartilage regions was observed in the UTE-AdiabT<sub>1ρ</sub> images with longer TSLs and the UTE-T<sub>2</sub><sup>\*</sup> images with longer TEs.

Figure 4 shows representative fitting curves and corresponding estimated UTE biomarkers for the OCJ, full cartilage, and superficial cartilage regions from a normal ex vivo knee sample. Excellent curve fittings were achieved for all techniques. The estimated T<sub>1</sub>, T<sub>1ρ</sub>, and T<sub>2</sub><sup>\*</sup> relaxation times of the OCJ region were much lower than those measured from the full cartilage and superficial cartilage regions, whereas the measured MMFs of the OCJ region were much higher than those obtained from the full thickness and superficial cartilage regions.

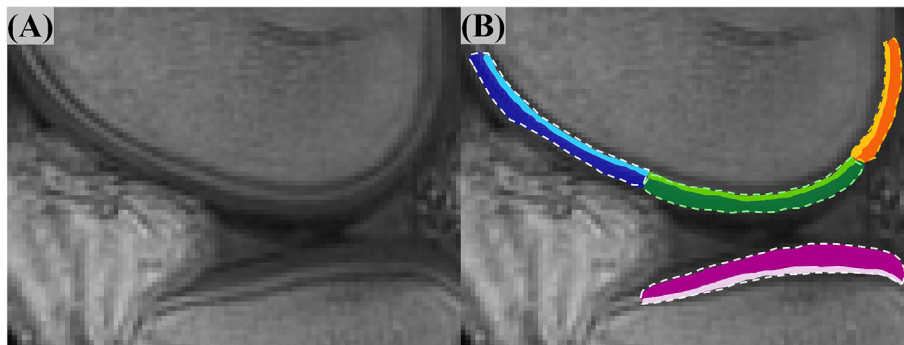


**FIGURE 3** Example of ROI delineation on a T<sub>1w</sub>-UTE image (FA = 30°) for a knee sample. The OCJ regions are highlighted as bright signal lines in this T<sub>1w</sub>-UTE image (A). The corresponding segmentations for the OCJ and superficial cartilage regions are presented in (B). Color-coded regions are described as follows: anterior femoral condyle (AFC) with blue color, inferior femoral condyle (IFC) with green color, posterior femoral condyle (PFC) with orange color, and tibial plateau (TP) with violet color. The regions in lighter shades denote the OCJ while regions in darker shades denote the superficial cartilage. The dashed lines denote full cartilage regions which are comprised of both superficial cartilage and the OCJ.

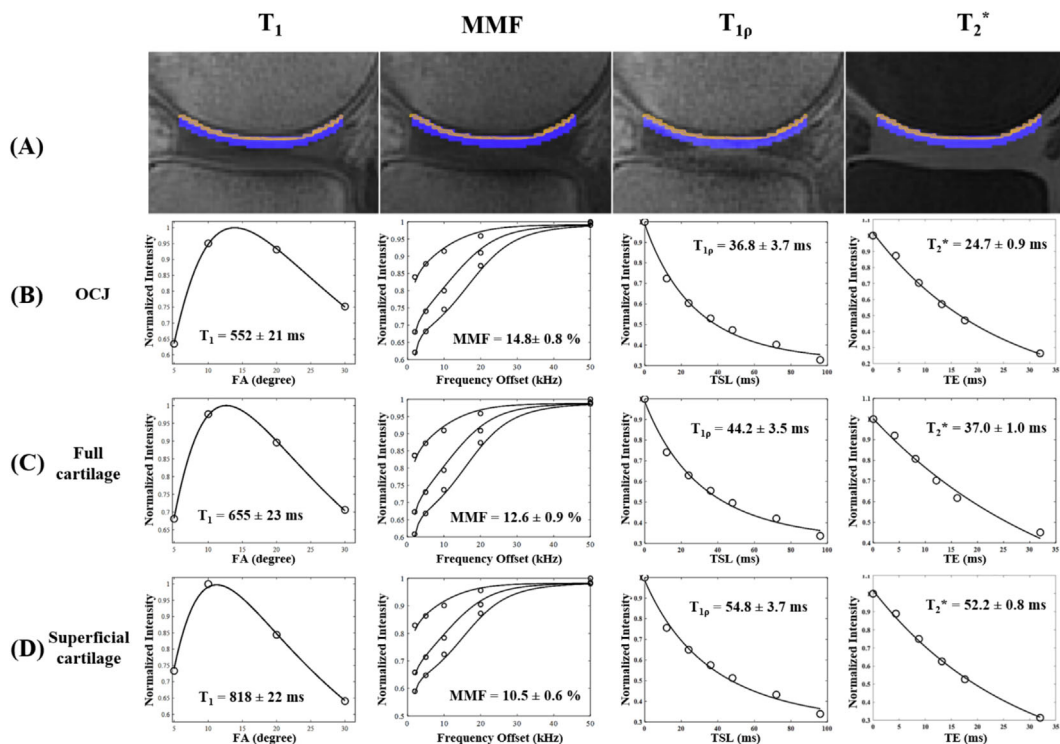


**FIGURE 4** Representative curve fitting for all four quantitative UTE techniques with ROIs drawn on the OCJ (orange region in (A)), superficial cartilage (blue region in (A)), and full cartilage (combined orange and blue regions in (A)) regions on a normal knee sample (45-year-old male donor). The fitting curves and corresponding estimated UTE biomarkers of T<sub>1</sub>, MMF, T<sub>1ρ</sub>, and T<sub>2</sub><sup>\*</sup> are presented from the first to fourth column respectively for OCJ (B), full cartilage (C), and superficial cartilage (D).

The UTE  $T_1$ , MMF,  $T_{1\rho}$ , and  $T_2^*$  measurements between the two readers showed high ICC values (respectively: 0.90, 0.90, 0.91, 0.88), indicating excellent reliability. The bar graphs of the measured quantitative UTE imaging biomarkers for different knee regions are displayed in Figure 5. Paired *t*-test results showed significant differences in all UTE measurements between the OCJ, full cartilage, and superficial cartilage regions for AFC, IFC, PFC, and TP parts (i.e., *p*-values less than 0.05). Similar to the results shown in Figure 4, the estimated  $T_1$ ,  $T_{1\rho}$ , and  $T_2^*$  values of all the OCJ regions were much lower than those measured from full cartilage and superficial cartilage regions, whereas the measured MMF values of the OCJ region were much higher than those obtained from the full cartilage and superficial cartilage regions. These regional differences for all the UTE biomarkers demonstrate a unique portfolio of properties for the OCJ region, potentially reflecting the variation of biochemical contents (e.g., water, collagen, and proteoglycan) across different cartilage layers. Table 1 summarizes the mean and standard deviation (SD) values for all the measurements as shown in Figure 5.

Figure 6 presents the clinical images (PD-FSE shown in Figures 6A,L and  $T_2$ -FSE shown in Figures 6B,M) and the parametric maps of UTE  $T_1$ , MMF,  $T_{1\rho}$ , and  $T_2^*$  from a normal knee joint sample (Figure 6D-G) and an abnormal knee joint sample (Figure 6H-K), respectively. As seen in the clinical MRI of the abnormal knee, the knee pathology involves chondral damage in the tibial plateau, specifically classified as Outerbridge grade I. As illustrated in the  $T_{1w}$ -UTE images (Figure 6C,N), the OCJ region presented as continuous bright signal lines in the normal knee sample, whereas the analogous OCJ region (indicated by arrows) in the abnormal knee showed a focal signal loss. Nearly all UTE biomarker maps showed higher values on the lesion region of the abnormal knee than those measured in the same anatomical region of the normal knee, except for MMF, which showed the reverse. Table 2 summarizes the UTE measurements of the OCJ, full cartilage, and superficial cartilage regions for the knee parts delineated by the yellow boxes shown in Figure 6D,H. The measured  $T_1$ ,  $T_{1\rho}$ , and  $T_2^*$  values of the OCJ, full cartilage, and superficial cartilage regions in the abnormal knee were higher than measurements in the corresponding regions of the normal sample, except for MMF which showed the reverse.

Table 3 summarizes the paired *t*-test *p*-values for different knee regions (AFC, PFC, IFC, and TP) across all quantitative UTE biomarkers. Most comparisons (35 out of 48) show significant differences. For the  $T_1$  biomarker, no significant differences are found between each of the two cartilage layers in the AFC region. However, significant differences are observed in the IFC, PFC, and TP regions. All biomarkers consistently show significance across all layers in the IFC region. A similar trend is observed in the TP region, except for the  $T_2^*$  biomarker when comparing the full and superficial layers. In the PFC region, the significance varies across different biomarkers. Despite these observations, a larger specimen cohort is necessary to draw more definitive conclusions.

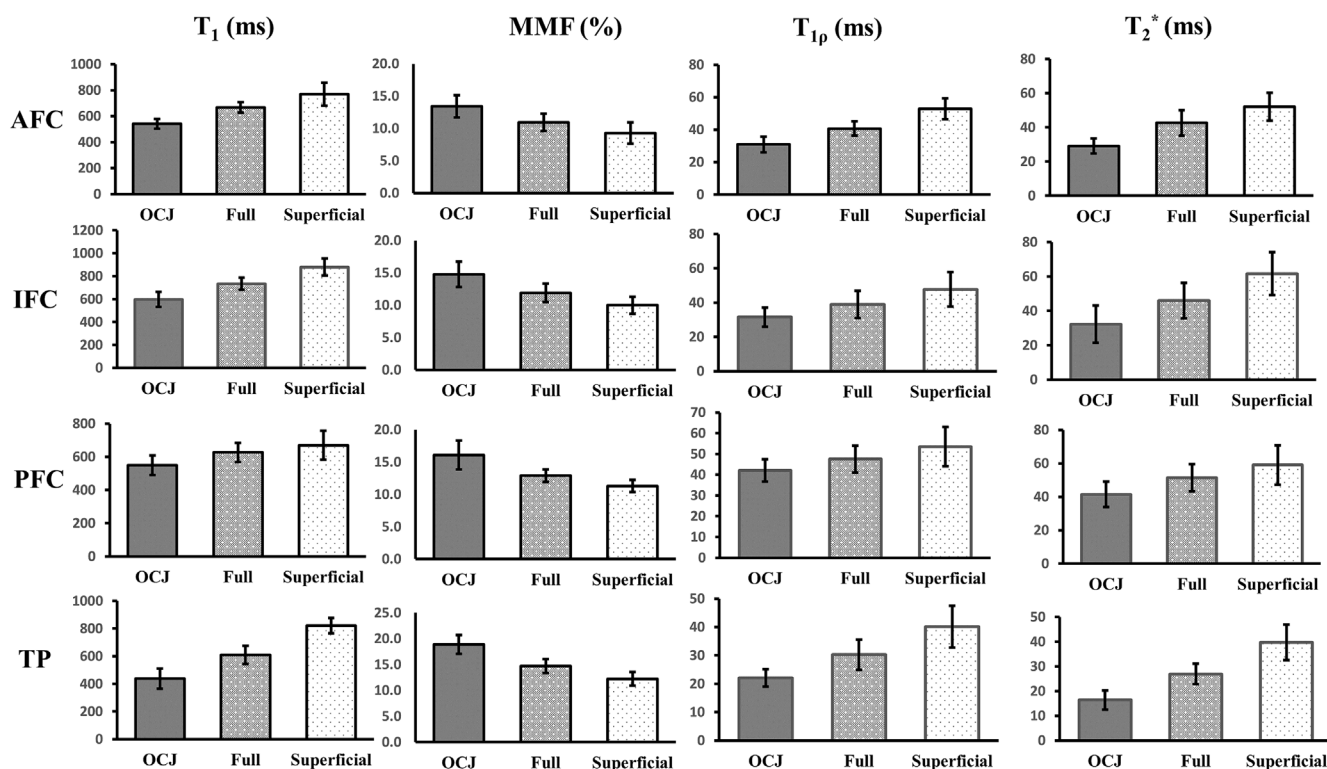


**FIGURE 5** Bar plots of UTE  $T_1$  (first column), MMF (second column),  $T_{1\rho}$  (third column), and  $T_2^*$  (fourth column) measurements on four different regions, namely the AFC (first row), IFC (second row), PFC (third row), and TP (fourth row), from 10 normal knee joint samples evaluated by a single reader. The quantitative UTE measures of the OCJ, full cartilage, and superficial cartilage regions for each knee part are plotted together for comparison. All UTE measurements showed significant differences between OCJ, full cartilage, and superficial cartilage regions for AFC, IFC, PFC, and TP parts.

**TABLE 1** Summarized quantitative UTE measurements of  $T_1$ , MMF,  $T_{1p}$ , and  $T_2^*$  (mean  $\pm$  SD) on OCJ, full cartilage, and superficial cartilage regions for AFC, IFC, PFC, and TP parts in 10 normal knee joint samples evaluated by a single reader.

		$T_1$ (ms)	MMF (%)	$T_{1p}$ (ms)	$T_2^*$ (ms)
OCJ	AFC	542 $\pm$ 38	13.2 $\pm$ 1.9	33.8 $\pm$ 4.8	29.0 $\pm$ 4.4
	IFC	623 $\pm$ 62	14.3 $\pm$ 1.6	36.4 $\pm$ 5.6	32.3 $\pm$ 5.8
	PFC	635 $\pm$ 71	13.6 $\pm$ 1.4	42.0 $\pm$ 5.4	55.3 $\pm$ 10.5
	TP	511 $\pm$ 57	17.7 $\pm$ 1.2	26.1 $\pm$ 3.1	17.2 $\pm$ 3.9
Full cartilage	AFC	667 $\pm$ 40	11.6 $\pm$ 1.2	43.3 $\pm$ 4.4	40.2 $\pm$ 7.4
	IFC	744 $\pm$ 64	11.4 $\pm$ 1.5	44.9 $\pm$ 7.9	46.0 $\pm$ 20.8
	PFC	707 $\pm$ 79	11.6 $\pm$ 1.1	47.5 $\pm$ 6.5	59.9 $\pm$ 10.4
	TP	659 $\pm$ 37	13.3 $\pm$ 1.6	35.7 $\pm$ 5.4	25.7 $\pm$ 4.2
Superficial cartilage	AFC	770 $\pm$ 79	10.6 $\pm$ 1.3	51.6 $\pm$ 6.5	48.3 $\pm$ 8.2
	IFC	884 $\pm$ 52	9.5 $\pm$ 1.3	55.3 $\pm$ 10.1	61.7 $\pm$ 15.8
	PFC	784 $\pm$ 96	10.1 $\pm$ 1.4	53.5 $\pm$ 9.6	65.2 $\pm$ 12.5
	TP	790 $\pm$ 39	11.1 $\pm$ 1.6	43.9 $\pm$ 7.5	32.4 $\pm$ 7.2

Abbreviations: AFC, anterior femoral condyle; IFC, inferior femoral condyle; OCJ, osteochondral junction; PFC, posterior femoral condyle; TP, tibial plateau.

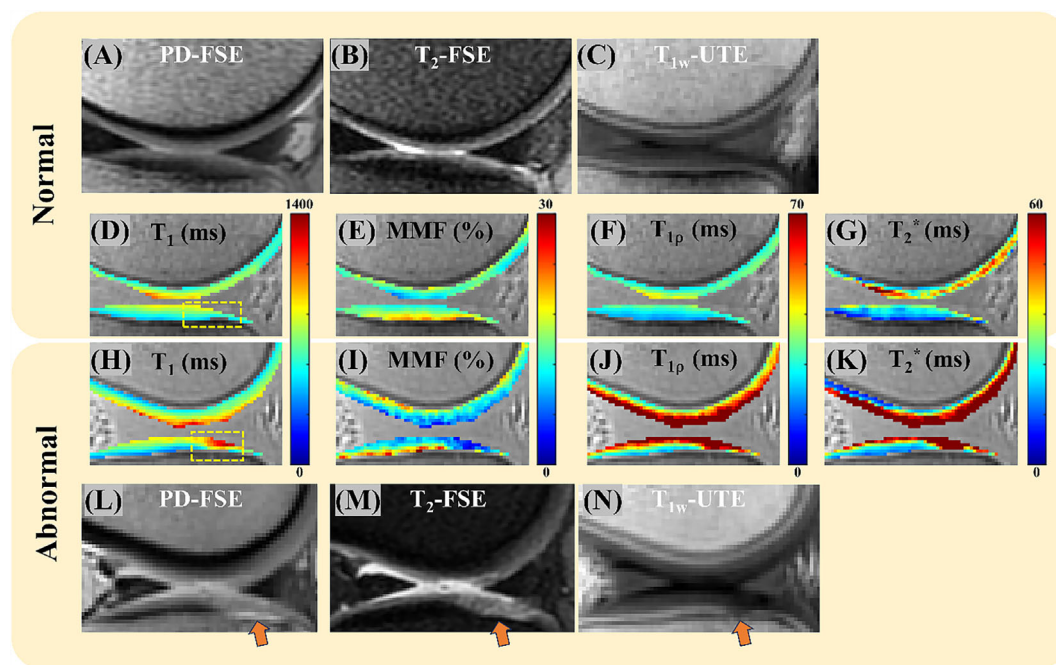


**FIGURE 6** Clinical imaging and quantitative UTE mapping of a normal knee sample from a 45-year-old male donor (A-G) and an abnormal knee sample from an 88-year-old male donor (H-N). The clinical PD-FSE (A and L) and T2-FSE (B and M) as well as  $T_{1w}$ -UTE (C and N) images are shown for morphological knee assessment. An abnormal cartilage region is indicated by arrows in the images from (L) to (N). OCJ signal loss of this lesion region is clearly seen in the  $T_{1w}$ -UTE image of the abnormal knee joint (N). Quantitative UTE  $T_1$  (D and H), MMF (E and I),  $T_{1p}$  (F and J), and  $T_2^*$  (G and K) maps for the normal and abnormal knee joints are shown for visual comparison. UTE measurements for regions inside the yellow dashed line boxes (see D and H) are found in Table 2.

## 4 | DISCUSSION

In this study, we investigated the feasibility of a comprehensive UTE imaging protocol in quantifying the OCJ region on ex vivo knee samples. The 3D UTE cones prototype sequence applied in this study had a nominal TE of 32  $\mu$ s, characteristic of UTE-type sequences that utilize TEs 100–1000 times shorter than those of conventional clinical sequences and allow for direct imaging and quantification of short  $T_2$  OCJ tissues. The proposed quantitative UTE imaging protocol, including UTE- $T_1$ , UTE-MT, UTE-Adiab $T_{1p}$ , and UTE- $T_2^*$ , successfully quantified  $T_1$ , MMF,  $T_{1p}$ , and  $T_2^*$



**TABLE 2** Mean and SD values of the quantitative UTE measurements of  $T_1$ , MMF,  $T_{1\rho}$ , and  $T_2^*$  for the cartilage lesion region in an abnormal knee sample from an 88-year-old male donor (yellow dashed line box in Figure 6H) and an analogous region of a normal knee sample from a 45-year-old male donor (yellow dashed line box in Figure 6D).

		$T_1$ (ms)	MMF (%)	$T_{1\rho}$ (ms)	$T_2^*$ (ms)
Normal	OCJ	519 ± 15	17.7 ± 1.1	22.2 ± 2.4	15.6 ± 0.3
	Full cartilage	623 ± 19	15.2 ± 0.9	26.5 ± 2.7	20.4 ± 0.2
	Superficial cartilage	774 ± 33	12.6 ± 0.7	32.6 ± 3.2	26.2 ± 1.3
Abnormal	OCJ	695 ± 18	8.7 ± 1.0	49.0 ± 11.4	45.8 ± 3.2
	Full cartilage	910 ± 17	5.6 ± 0.6	71.7 ± 21.2	73.5 ± 5.7
	Superficial cartilage	1135 ± 35	4.8 ± 0.4	93.1 ± 30.0	108.9 ± 11.8

Abbreviation: OCJ, osteochondral junction.

**TABLE 3** Summarized  $p$ -values for pairwise comparisons between three cartilage layers (OCJ, full cartilage, and superficial cartilage) for four biomarkers ( $T_1$ , MMF,  $T_{1\rho}$ , and  $T_2^*$ ) across four different knee regions (AFC, PFC, IFC, and TP) in 10 normal knee joint samples.

	OCJ vs. full	Full vs. superficial	OCJ vs. superficial
		IFC	
$T_1$	0.001	0.006	0.003
$T_{1\rho}$	*	*	*
MMF	0.002	*	0.001
$T_2^*$	*	0.001	*
		IFC	
$T_1$	*	*	*
$T_{1\rho}$	*	*	*
MMF	*	*	*
$T_2^*$	*	*	*
		PFC	
$T_1$	*	*	*
$T_{1\rho}$	*	0.005	0.001
MMF	0.002	0.001	*
$T_2^*$	*	0.016	0.002
		TP	
$T_1$	*	*	*
$T_{1\rho}$	*	*	*
MMF	*	*	*
$T_2^*$	*	0.009	*

Abbreviations: AFC, anterior femoral condyle; IFC, inferior femoral condyle; OCJ, osteochondral junction; PFC, posterior femoral condyle; TP, tibial plateau.

\*Statistical significance (i.e.,  $p < 0.001$ ).

[Correction added on 10 September 2024, after first online publication: the format of Table 3 was incorrect and was corrected in this version.]

for the OCJ, full thickness, and superficial cartilage regions for different anatomical areas, namely, the AFC, IFC, PFC, and TP. All UTE biomarkers revealed significant differences between the OCJ and the full thickness or superficial cartilage regions, with lower  $T_1$ ,  $T_{1\rho}$ , and  $T_2^*$  values but higher MMF values in the OCJ compared with either the full thickness or superficial cartilage region. Substantial differences were also observed for all UTE measurements in the OCJ region between normal and abnormal cartilage regions. These results together demonstrate the feasibility of quantifying OCJ region using the proposed UTE imaging protocol on ex vivo knee samples.

OA is known to be a primary cause of chronic pain and disability in the aging population,<sup>47</sup> and the OCJ region has been identified to play a vital role in the disease's pathogenesis and symptoms<sup>11</sup>: a healthy joint depends on the integrity of this region, and its impairment is characteristic of OA. Quantitative evaluation of compositional changes that may occur in the OCJ region could therefore reveal OA disease progression in a clinically relevant way. The proposed comprehensive UTE imaging protocol provides a quantitative evaluation of the short  $T_2$  OCJ regions for the assessment of injuries or degenerative changes, including quantifiable alterations in the proteoglycan, collagen matrix, and water content.

The OCJ region exhibited significantly lower UTE  $T_1$ ,  $T_{1\rho}$ , and  $T_2^*$  measures compared with both the full cartilage and superficial cartilage regions. Conversely, the measured MMFs in the OCJ region were notably higher in comparison with the other two regions. These results could be attributed to not only the high collagen density and integrity of the deep layers of cartilage but also their calcification. Results also showed that the measured  $T_1$ ,  $T_{1\rho}$ , and  $T_2^*$  values of the abnormal OCJ region were much higher than these measurements in the corresponding normal region, whereas MMF showed the opposite trend. These results demonstrate that quantitative imaging of the OCJ region using the proposed UTE protocol is promising in studying the biochemical contents and assessing their changes clinically.

UTE- $T_2^*$  has been used to quantify cartilage in several studies, suggesting its utility in facilitating the detection of early degenerative changes. As reported in Williams et al.,<sup>48</sup> UTE- $T_2^*$  mapping of articular cartilage was found to be sensitive to matrix degeneration. This study also demonstrated the advantage of UTE- $T_2^*$  mapping for the assessment of short  $T_2$  deep zone cartilage regions as opposed to standard  $T_2$  mapping. Another in vivo cartilage study<sup>49</sup> demonstrated high repeatability with the UTE- $T_2^*$  technique and found that UTE- $T_2^*$  values were higher in superficial cartilage than deep cartilage, a result aligned with our findings. Furthermore, clinical translational studies showed that patients with ACL reconstruction demonstrated increased UTE- $T_2^*$  values within the deep patellar cartilage compared with control subjects.<sup>31,32</sup> Our observations comparing normal knee joints to abnormal knee joints closely mirror the outcomes reported above. Although prior investigations primarily centered on UTE- $T_2^*$ , our proposed UTE imaging protocol has the potential to offer a thorough assessment of the compositional changes in the OCJ region, encompassing a broader scope with regard to the evaluation of whole joint systems.

This work primarily focuses on investigating the feasibility of OCJ imaging using the proposed comprehensive UTE protocol. There were several limitations in this study. First, there was only a single specimen in the abnormal group, precluding any statistical comparison between normal and OA cohorts. We plan to scan large cohorts of OA patients in the future to validate the clinical value of the proposed OCJ imaging protocol for OA assessment. Second, no comparison between UTE biomarkers and histological staining on the OCJ region was performed, a validation phase that will be established in a future study. Third, the scan time of the proposed protocol is very long (~90 min) and will be accelerated using parallel imaging and compressed sensing<sup>50,51</sup> for future in vivo studies.

## 5 | CONCLUSION

The proposed comprehensive UTE imaging protocol can feasibly quantify the short  $T_2$  OCJ region in the knee joint, showing promise for studying knee OA.

### ACKNOWLEDGMENTS

The authors acknowledge grant support from the National Institutes of Health (R01AR062581, R01AR068987, R01AR075825, R01AR078877, R01AR079484, P30AR073761, R21AR075851, and F32AG082458), the VA Clinical Science Research & Development Service (I01CX001388 and I01CX000625), and GE Healthcare.

### CONFLICT OF INTEREST STATEMENT

The authors have no conflicts of interest to declare.

### DATA AVAILABILITY STATEMENT

The data that support the findings of this study are available on request from the corresponding author. The data are not publicly available due to privacy or ethical restrictions.

### ORCID

Jiyo S. Athertya  <https://orcid.org/0000-0002-0866-1052>

Alecio F. Lombardi  <https://orcid.org/0000-0002-6820-1779>

Dina Moazamian  <https://orcid.org/0000-0002-8815-4535>

### REFERENCES

- Loeser RF, Goldring SR, Scanzello CR, Goldring MB. Osteoarthritis: a disease of the joint as an organ. *Arthritis Rheum*. 2012;64(6):1697-1707. doi:10.1002/art.34453
- Yuan XL, Meng HY, Wang YC, et al. Bone-cartilage interface crosstalk in osteoarthritis: potential pathways and future therapeutic strategies. *Osteoarthr Cartil*. 2014;22(8):1077-1089. doi:10.1016/j.joca.2014.05.023
- Mapp PI, Walsh DA. Mechanisms and targets of angiogenesis and nerve growth in osteoarthritis. *Nat Rev Rheumatol*. 2012;8(7):390-398. doi:10.1038/nrrheum.2012.80
- Goldring SR. Alterations in periarticular bone and cross talk between subchondral bone and articular cartilage in osteoarthritis. *Ther Adv Musculoskelet Dis*. 2012;4(4):249-258. doi:10.1177/1759720X12437353

5. Oegema TR, Carpenter RJ, Hofmeister F, Thompson RC. The interaction of the zone of calcified cartilage and subchondral bone in osteoarthritis. *Microsc Res Tech*. 1997;37(4):324-332. doi:10.1002/(SICI)1097-0029(19970515)37:43.O.CO;2-K
6. Walsh DA, McWilliams DF, Turley MJ, et al. Angiogenesis and nerve growth factor at the osteochondral junction in rheumatoid arthritis and osteoarthritis. *Rheumatology*. 2010;49(10):1852-1861. doi:10.1093/rheumatology/keq188
7. Walsh DA, Bonnet CS, Turner EL, Wilson D, Situ M, McWilliams DF. Angiogenesis in the synovium and at the osteochondral junction in osteoarthritis. *Osteoarthr Cartil*. 2007;15(7):743-751. doi:10.1016/j.joca.2007.01.020
8. Intema F, Hazewinkel HAW, Gouwens D, et al. In early OA, thinning of the subchondral plate is directly related to cartilage damage: results from a canine ACLT-menisectomy model. *Osteoarthr Cartil*. 2010;18(5):691-698. doi:10.1016/j.joca.2010.01.004
9. Suri S, Gill SE, De Camin SM, Wilson D, McWilliams DF, Walsh DA. Neurovascular invasion at the osteochondral junction and in osteophytes in osteoarthritis. *Ann Rheum Dis*. 2007;66(11):1423-1428. doi:10.1136/ard.2006.063354
10. Findlay DM, Atkins GJ. Osteoblast-chondrocyte interactions in osteoarthritis. *Curr Osteoporos Rep*. 2014;12(1):127-134. doi:10.1007/s11914-014-0192-5
11. Suri S, Walsh DA. Osteochondral alterations in osteoarthritis. *Bone*. 2012;51(2):204-211. doi:10.1016/j.bone.2011.10.010
12. Guermazi A, Roemer FW, Hayashi D. Imaging of osteoarthritis: update from a radiological perspective. *Curr Opin Rheumatol*. 2011;23(5):484-491. doi:10.1097/BOR.0b013e328349c2d2
13. Regatte RR, Akella SVS, Lonner JH, Kneeland JB, Reddy R. T1p mapping in human osteoarthritis (OA) cartilage: comparison of T1p with T2. *J Magn Reson Imaging*. 2006;23(4):547-553. doi:10.1002/jmri.20536
14. Wang L, Regatte RR. T1p MRI of human musculoskeletal system. *J Magn Reson Imaging*. 2015;41(3):586-600. doi:10.1002/jmri.24677
15. Prasad AP, Nardo L, Schooler J, Joseph GB, Link TM. T1p and T2 relaxation times predict progression of knee osteoarthritis. *Osteoarthr Cartil*. 2013;21(1):69-76. doi:10.1016/j.joca.2012.09.011
16. Wolff SD, Balaban RS. Magnetization transfer contrast (MTC) and tissue water proton relaxation in vivo. *Magn Reson Med*. 1989;10(1):135-144. doi:10.1002/mrm.1910100113
17. Sled JG, Bruce PG. Quantitative imaging of magnetization transfer exchange and relaxation properties in vivo using MRI. *Magn Reson Med*. 2001;46(5):923-931. doi:10.1002/mrm.1278
18. Henkelman RM, Stanisz GJ, Graham SJ. Magnetization transfer in MRI: a review. *NMR Biomed*. 2001;14(2):57-64. doi:10.1002/nbm.683
19. Ma Y, Jang H, Jerban S, et al. Making the invisible visible - ultrashort echo time magnetic resonance imaging: technical developments and applications. *Appl Phys Rev*. 2022;9(4):41303. doi:10.1063/5.0086459
20. Sedaghat S, Jang H, Ma Y, et al. Clinical evaluation of white matter lesions on 3D inversion recovery ultrashort echo time MRI in multiple sclerosis. *Quant Imaging Med Surg*. 2023;13(7). doi:10.21037/qims-22-1317
21. Afsahi AM, Ma Y, Jang H, et al. Ultrashort echo time magnetic resonance imaging techniques: met and unmet needs in musculoskeletal imaging. *J Magn Reson Imaging*. Published online December. 2021;55(6):1-16. doi:10.1002/jmri.28032
22. Malhi BS, Moazamian D, Shin SH, et al. Bi-exponential 3D UTE-T1p relaxation mapping of ex vivo human knee patellar tendon at 3T. *Bioengineering*. 2024;11(1):66. doi:10.3390/bioengineering11010066
23. Afsahi AM, Sedaghat S, Moazamian D, et al. Articular cartilage assessment using ultrashort echo time MRI: a review. *Front Endocrinol (Lausanne)*. 2022;13(May):1-17. doi:10.3389/fendo.2022.892961
24. Lombardi AF, Guma M, Chung CB, Chang EY, Du J, Ma YJ. Ultrashort echo time magnetic resonance imaging of the osteochondral junction. *NMR Biomed*. 2023;36(2):1-19. doi:10.1002/nbm.4843
25. Bae WC, Dwek JR, Znamirovski R, et al. Ultrashort echo time MR imaging of osteochondral junction of the knee at 3 T: identification of anatomic structures contributing to signal intensity. *Radiology*. 2010;254(3):837-845. doi:10.1148/radiol.09081743
26. Du J, Bydder M, Takahashi AM, Carl M, Chung CB, Bydder GM. Short T2 contrast with three-dimensional ultrashort echo time imaging. *Magn Reson Imaging*. 2011;29(4):470-482. doi:10.1016/j.mri.2010.11.003
27. Liu J, Wei Y, Ma YJ, Zhu YC, Zhou Q, Zhao YH. Magnetic resonance imaging of the zone of calcified cartilage in the knee joint using 3-dimensional ultrashort echo time cones sequences. *Chin Med J (Engl)*. 2019;132(5):562-568. doi:10.1097/CM9.000000000000103
28. Cai Z, Wei Z, Wu M, et al. Knee osteochondral junction imaging using a fast 3D T1-weighted ultrashort echo time cones sequence at 3T. *Magn Reson Imaging*. 2020;73(February):76-83. doi:10.1016/j.mri.2020.08.003
29. Ma YJ, Jerban S, Carl M, et al. Imaging of the region of the osteochondral junction (OCJ) using a 3D adiabatic inversion recovery prepared ultrashort echo time cones (3D IR-UTE-cones) sequence at 3 T. *NMR Biomed*. 2019;32(5):1-13. doi:10.1002/nbm.4080
30. Lombardi AF, Jang H, Wei Z, et al. High-contrast osteochondral junction imaging using a 3D dual adiabatic inversion recovery-prepared ultrashort echo time cones sequence. *NMR Biomed*. 2021;34(8):1-11. doi:10.1002/nbm.4559
31. Williams AA, Erhart-Hledik JC, Asay JL, et al. Patient-reported outcomes and knee mechanics correlate with patellofemoral deep cartilage UTE-T2\* 2 years after anterior cruciate ligament reconstruction. *Am J Sports Med*. 2021;49(3):675-683. doi:10.1177/0363546520982608
32. Titchenal MR, Williams AA, Chehab EF, et al. Cartilage subsurface changes to magnetic resonance imaging UTE-T2\* 2 years after anterior cruciate ligament reconstruction correlate with walking mechanics associated with knee osteoarthritis. *Am J Sports Med*. 2018;46(3):565-572. doi:10.1177/0363546517743969
33. Fram EK, Herfkens RJ, Johnson GA, et al. Rapid calculation of T1 using variable flip angle gradient refocused imaging. *Magn Reson Imaging*. 1987;5(3):201-208. doi:10.1016/0730-725X(87)90021-X
34. Ma YJ, Zhao W, Wan L, et al. Whole knee joint T1 values measured in vivo at 3T by combined 3D ultrashort echo time cones actual flip angle and variable flip angle methods. *Magn Reson Med*. 2019;81(3):1634-1644. doi:10.1002/mrm.27510
35. Ma YJ, Chang EY, Carl M, Du J. Quantitative magnetization transfer ultrashort echo time imaging using a time-efficient 3D multispoke cones sequence. *Magn Reson Med*. 2018;79(2):692-700. doi:10.1002/mrm.26716
36. Michaeli S, Sorce DJ, Springer CS, Ugurbil K, Garwood M. T1p MRI contrast in the human brain: modulation of the longitudinal rotating frame relaxation shutter-speed during an adiabatic RF pulse. *J Magn Reson*. 2006;181(1):135-147. doi:10.1016/j.jmr.2006.04.002
37. Ma YJ, Carl M, Searleman A, Lu X, Chang EY, Du J. 3D adiabatic T1p prepared ultrashort echo time cones sequence for whole knee imaging. *Magn Reson Med*. 2018;80(4):1429-1439. doi:10.1002/mrm.27131

38. Chen B, Zhao Y, Cheng X, et al. Three-dimensional ultrashort echo time cones (3D UTE-cones) magnetic resonance imaging of entheses and tendons. *Magn Reson Imaging*. 2018;49(December 2017):4-9. doi:[10.1016/j.mri.2017.12.034](https://doi.org/10.1016/j.mri.2017.12.034)
39. Yarnykh VL. Actual flip-angle imaging in the pulsed steady state: a method for rapid three-dimensional mapping of the transmitted radiofrequency field. *Magn Reson Med*. 2007;57(1):192-200. doi:[10.1002/mrm.21120](https://doi.org/10.1002/mrm.21120)
40. Bydder M, Rahal A, Fullerton GD, Bydder GM. The magic angle effect: a source of artifact, determinant of image contrast, and technique for imaging. *J Magn Reson Imaging*. 2007;25(2):290-300. doi:[10.1002/jmri.20850](https://doi.org/10.1002/jmri.20850)
41. Ma YJ, Shao H, Du J, Chang EY. Ultrashort echo time magnetization transfer (UTE-MT) imaging and modeling: magic angle independent biomarkers of tissue properties. *NMR Biomed*. 2016;29(11):1546-1552. doi:[10.1002/nbm.3609](https://doi.org/10.1002/nbm.3609)
42. Hänninen N, Rautiainen J, Rieppo L, Saarakkala S, Nissi MJ. Orientation anisotropy of quantitative MRI relaxation parameters in ordered tissue. *Sci Rep*. 2017;7(1):9606. doi:[10.1038/s41598-017-10053-2](https://doi.org/10.1038/s41598-017-10053-2)
43. Kantola V, Karjalainen J, Jaakola T, et al. Anisotropy of T2 and T1 $\rho$  relaxation time in articular cartilage at 3 T. *Magn Reson Med*. 2024;(March):1-12. doi:[10.1002/mrm.30096](https://doi.org/10.1002/mrm.30096)
44. Gurney PT, Hargreaves BA, Nishimura DG. Design and analysis of a practical 3D cones trajectory. *Magn Reson Med*. 2006;55(3):575-582. doi:[10.1002/mrm.20796](https://doi.org/10.1002/mrm.20796)
45. Levenberg K. A method for the solution of certain non-linear problems in least squares. *Q Appl Math* 1944;2(2):164-168. <http://www.jstor.org/stable/43633451>
46. Marquardt DW. An algorithm for least-squares estimation of nonlinear parameters. *J Soc Ind Appl Math* 1963;11(2):431-441. <http://www.jstor.org/stable/2098941>
47. Anderson AS, Loeser RF. Why is OA an age-related disease. *Best Pr Res Clin Rheumatol*. 2010;24(1):1-18. doi:[10.1016/j.berh.2009.08.006](https://doi.org/10.1016/j.berh.2009.08.006). Why
48. Williams A, Qian Y, Bear D, Chu CR. Assessing degeneration of human articular cartilage with ultra-short echo time (UTE) T2\* mapping. *Osteoarthr Cartil*. 2010;18(4):539-546. doi:[10.1016/j.joca.2010.02.001](https://doi.org/10.1016/j.joca.2010.02.001)
49. Williams A, Qian Y, Chu CR. UTE-T2\* mapping of human articular cartilage in vivo: a repeatability assessment. *Osteoarthr Cartil*. 2011;19(1):84-88. doi:[10.1016/j.joca.2010.10.018](https://doi.org/10.1016/j.joca.2010.10.018)
50. Lustig M, Donoho DL, Santos JM, Pauly JM. Compressed sensing MRI: a look at how CS can improve on current imaging techniques. *IEEE Signal Process Mag*. 2008;25(2):72-82. doi:[10.1109/MSP.2007.914728](https://doi.org/10.1109/MSP.2007.914728)
51. Wang S, Su Z, Ying L, et al. Accelerating magnetic resonance imaging via deep learning. In: *IEEE 13th International Symposium on Biomedical Imaging (ISBI)*. Vol.2016. IEEE; 2016:514-517. doi:[10.1109/ISBI.2016.7493320](https://doi.org/10.1109/ISBI.2016.7493320)

**How to cite this article:** Athertya JS, Suprana A, Lo J, et al. Quantitative ultrashort echo time MR imaging of knee osteochondral junction: An ex vivo feasibility study. *NMR in Biomedicine*. 2024;37(12):e5253. doi:[10.1002/nbm.5253](https://doi.org/10.1002/nbm.5253)